RSC Advances

PAPER

Cite this: *RSC Adv.*, 2019, **9**, 32608

Density functional study of Li/Na adsorption properties of single-layer and double-layer antimonenes

Huilan Wei, Jianping Sun,* Yifan Hu, Zhao Li and Mei Ai

Received 4th August 2019
Accepted 19th September 2019

DOI: 10.1039/c9ra06059f

rsc.li/rsc-advances

β-Antimonene, a stable two-dimensional material, has been successfully prepared recently. Experiments have demonstrated β-antimonene's excellent Li storage properties. Based on first-principles density functional theory (DFT), the adsorption properties of Li/Na atoms on single-layer antimonene (SL-Sb) and double-layer antimonene (DL-Sb) have been studied. The optimal adsorption position of Li/Na atoms on SL-Sb is the V site with an adsorption energy of 1.91/1.46 eV. With the increase of Li adsorption density, the crystal structure of the antimonene changes significantly. The optimal adsorption position of Li on DL-Sb is the V2 site in the interlayer with an adsorption energy of 2.71 eV, and that of Na is the V1 site outside the surface with an adsorption energy of 1.72 eV. With the increase of the adsorption density of Li, the antimonene presented a trend of forming an alloy. Whereas with the increase of Na adsorption density, the antimonene retains its original structure. The diffusion barrier of Li/Na atoms on the SL-Sb surface is 0.22/0.13 eV, and outside the DL-Sb surface is 0.25/0.15 eV. In short, DL-Sb can maintain a stable structure with a large Li/Na storage density; the diffusion barriers of Li/Na atoms on antimonene are relatively low, which is beneficial to the rapid insertion/extraction.

1 Introduction

Lithium-ion batteries (LIBs) are widely used in portable electronic devices and communication facilities due to their high reversible capacity, high energy density and good cycle life.[1] With the prevalence of electric vehicles and the rapid development of electric energy storage systems, higher requirements have been put forward for the energy storage density, output power and charging and discharging rate of LIBs. In addition, due to the limited reserves and high price of lithium resources, research on Na ion, Al ion and other batteries have attracted more interest.[2] Na is adjacent to Li in the periodic table of elements, and is abundant on earth, sharing many similar characteristics with alkali metal elements. Therefore, sodium-ion battery (NIB) technology is expected to be employed in large-scale energy storage.[3] The anode material has an essential influence on the performance of secondary ion batteries. Superior anode materials should have high storage capacity, low oxidation–reduction potential, high ion diffusion rate and good stability.[4] Graphite, as a common anode material of LIBs, has excellent electrical properties and chemical stability. However, the storage capacity of graphite is close to the theoretical limit. For Na storage, Rytkönen *et al.* found that Na atoms tend to form Na_3, Na_4 and Na_5 clusters on the graphite surface by using the GGA-PBE theoretical method.[5] Other carbon-based structures such as hard carbon, porous carbon, and porous layered oxide materials (TiO_2, *etc.*) have also been studied.[6,7] In order to improve the storage density, bulk materials such as Si, Sn, Ge and Sb have been studied. It is found that these materials have a high Li/Na storage capacity, but undergoing a dramatic volume change during the process of inserting/extracting Li/Na, which leads to pulverization of the electrode materials.[8,9]

Compared with bulk materials, two-dimensional materials have a large surface area and weak van der Waals interaction between layers, which can reduce the volume expansion and contraction caused by ions insertion/extraction.[8,10] Graphene is a typical two-dimensional material, whose research as anode material of LIBs has received extensive attention. Yoo *et al.* reported in 2008 that graphene was directly used as a anode material for LIBs with a specific capacity of 540 mA h g^{-1}.[11] Zheng *et al.* found that the diffusion barrier of Li atoms on the graphene surface was only 0.32 eV, and through the carbon ring was as high as 10.68 eV.[12] In order to improve the storage performance of graphene, methods such as doping graphene and constructing heterostructure between graphene and other two-dimensional materials have been adopted. Ling *et al.* pointed out that the adsorption of Na on the surface of graphene was thermodynamically unstable, and the adsorption capacity of graphene could be improved by doping boron.[13] Some studies have shown that heterostructures can effectively utilize the advantages of both

School of Electrical and Electronic Engineering, North China Electric Power University, Beijing 102206, China. E-mail: sunjp@ncepu.edu.cn

materials to enhance the adsorption ability and structure stability. Shi *et al.* used 2 × 2 silicene supercells and 3 × 3 graphene supercells to construct heterostructure, and found that the graphene/silicene heterostructure preserved the characteristics of silicene with high specific capacity and low diffusion barrier.[10] Using the GGA-PBE method, Chen *et al.* constructed the TiO_2/graphene heterostructure and obtained that the diffusion barrier of Na on the heterostructure was 0.2 eV, which was conducive to Na diffusion.[14]

In addition to graphene, other two-dimensional materials are also studied. The borophene has high specific capacity and good Li/Na diffusion performance,[15,16] but preparing borophene require ultra-high vacuum.[17] The Bohayra *et al.* studied silicene, germanene, and stanene, with high Li/Na specific capacity of 954, 369, and 226 mA h g^{-1}, respectively, but after adsorption of the atoms, the structure will be deformed and the intercalation degraded.[8] Huang *et al.* used transmission electron microscopy to explore the structure and phase transitions of few-layer bismuthene during Na intercalation. They found that the phase transitions from NaBi to c-Na_3Bi (cubic), and finally to h-Na_3Bi (hexagonal), meanwhile, the 2D feature of bismuthene can still retain after repeated sodiation/desodiation processes, suggesting that bismuthene can alleviate the huge volume expansion of alloying processes.[18] Phosphene has excellent ion storage characteristics and low diffusion barrier. It is reported that single-layer blue-phosphene and black-phosphene can adsorb a large amount of Li ions, and the diffusion barrier is lower than 0.8 eV.[19,20] Liu *et al.* calculated the specific capacities of Na adsorbed phosphene by DFT-D2 and DFT methods, which were 865 mA h g^{-1} and 433 mA h g^{-1}, respectively.[21] Hembram *et al.* constructed a 2 × 2 × 2 black phosphorus supercell to adsorb Li, Na and Mg atoms. The configurations that could adsorb the most atoms were $Li_{4.5}P$, $Na_{4.0}P$ and $Mg_{2.0}P$, respectively.[22,23] Phosphene has a very high Li/Na storage capacity, however it is easy to oxidize in air with poor stability.[24,25]

Recently, a new two-dimensional material, β-antimonene, was successfully prepared, which has attracted researchers' attention.[26,27] It is stable in air, and has unique physical and chemical properties. Huo *et al.* provided a highly efficient and stable liquid phase exfoliation method to extract few-layer antimonene. The obtained few-layer antimonene was found to be stable in the ambient environment with good optical properties.[28] Carlos[29] *et al.* and Abellan[30] *et al.* prepared suspension of micrometer size few-layer antimonene by sonication in isopropanol/water mixture without surfactant. Gao *et al.* prepared Sb nanoparticles and few-layer antimonene by regulating ultrasonication.[31] Tao *et al.* produced stable bilayer antimonene on Bi_2Te_3 and Sb_2Te_3 substrates.[32] In addition to antimonene, the researches on other 2D VA monoelemental and bielemental structures, such as such as bismuthene and BiSb, have been carried out.[33,34] Previously, many studies were conducted on the storage of Li/Na in bulk Sb. Bulk Sb can form Li_3Sb/Na_3Sb with Li/Na, and the theoretical specific capacity is 660 mA h g^{-1}.[35] In 2012, Qian *et al.* reported the research on sodium storage of Sb/C composite structure, which showed a reversible capacity of 610 mA h g^{-1} at 100 mA g^{-1}.[36] Zhang *et al.* reported a dealloying synthetic strategy to prepare bismuth-antimony anodes for NIBs, and found that the nanoporous Bi_2Sb_6 alloy exhibited an ultralong cycling performance (10 000 cycles) at 1 A g^{-1} corresponding to a capacity decay of merely 0.0072% per cycle.[37] Hopefully, antimonene could weaken the influence of the volume expansion, and improve the cycle life of the battery. Experimentally, Gao *et al.* tested the cycle performance of bulk Sb, antimonene and Sb nanoparticles (NPs) for Li ions storage at a current density of 0.5C (1C = 660 mA h g^{-1}). The bulk Sb decayed rapidly after a dozen cycles, while the antimonene only decayed by 3.8% after 100 charged and discharged cycles, and the Sb NPs decayed by 21.9% after 100 cycles. Among the three structures, antimonene exhibited the best cycling properties. The diffusion barrier of Li^+ on the surface of the antimonene is only 0.25 eV.[31] In theoretical calculations, Amretashis *et al.* constructed a single layer of 4 × 4 antimonene supercells to study Li/Na adsorption properties. The antimonene can adsorb 32 Li atoms or 64 Na (theoretical specific capacities are 208 mA h g^{-1} and 320 mA h g^{-1}, respectively), and the diffusion barrier of Li/Na is 0.337/0.114 eV.[38] The experiments have demonstrated that antimonene has a good potential for Li storage, however, the systematic theoretical study of antimonene as Li/Na ion electrode material is still lacking.

Based on density functional theory (DFT), the properties of single-layer and double-layer β-antimonene adsorbing Li/Na have been systematically studied in this paper. In single-layer antimonene (SL-Sb), the adsorption configuration and stability have been investigated. Because few-layer antimonenes are more likely to be the practical materials, the double-layer antimonene (DL-Sb) was adopted as model of few-layer antimonene for study. The adsorption of Li/Na on DL-Sb is more stable than that on SL-Sb. In addition, the diffusion of Li and Na atoms on SL-Sb and DL-Sb have been investigated, showing that the diffusion barrier of Li/Na on SL-Sb is 0.22/0.13 eV, which is lower than on DL-Sb surface (0.25/0.15 eV) and in DL-Sb interlayer (1.11/0.65 eV). The findings show that DL-Sb is a promising candidate for the anode material of lithium/sodium ion batteries.

2 Computational methodology

All the calculations performed in this paper are based on density functional theory (DFT) as implemented in the Vienna *ab initio* simulation package (VASP).[39,40] We use generalized gradient approximation (GGA) with the parametrization of Perdew–Burke–Ernzerhof (PBE). The empirical correction scheme of Grimme (DFT + D2) for van der Waals interaction was adopted. The cutoff energy used in structural optimization and static calculation has been tested, and 500 eV is adopted. A 5 × 5 × 1 Monkhorst–Pack mesh is used for relaxation calculations and a 11 × 11 × 1 Monkhorst–Pack mesh is used for static electronic structure calculations. Geometry structures are relaxed until the force on each atom is less than 0.01 eV $Å^{-1}$, and the energy convergence criteria is 1 × 10^{-4} eV. A vacuum space of 20 Å in the *Z* direction is used to avoid the interaction between the periodically repeated structures. It is found that there is no spin polarization between the Sb atoms and the Li/

Na atoms, so the spin polarization is not considered in the calculation. We used a 4 × 4 supercell for single-layer antimonene (32 Sb atoms) and a 3 × 3 supercell for double-layer antimonene (36 Sb atoms).

The adsorption energy of Li/Na atom is defined as:

$$E_{ad} = E_{antimonene} + E_{Li/Na} - E_{antimonene+Li/Na} \quad (1)$$

where $E_{antimonene}$ is the total energy of the pristine SL-Sb/DL-Sb, $E_{Li/Na}$ is the energy of single Li/Na atom, and $E_{antimonene+Li/Na}$ is the total energy of SL-Sb/DL-Sb with the adsorbed Li/Na atom. When the calculation result is positive, a larger value means stronger adsorption.

In order to study the diffusion behavior of Li/Na in antimonene, we use the standard nudged elastic band method (NEB).[41] Firstly, the initial state and final state of the adsorbed atom are determined. Then, 5 intermediate states are inserted between them to find the diffusion path. Finally, the maximum value of energy in the five states is found after relaxation calculation. The difference between the maximum energy and the initial energy is the diffusion barrier.

Open circuit voltage (OCV) is an important figure of merit that can characterize the performance of ion batteries, thus we calculate the OCV in this paper. The average voltage is defined as:[42,43]

$$V \approx -\frac{E_{x_2} - E_{x_1} - (x_2 - x_1)E_{Li/Na}}{(x_2 - x_1)e} \quad (2)$$

where E_x is the total energy of the adsorbing system (Li_xSb, Na_xSb), $E_{Li/Na}$ is the Li/Na atom energy in the bulk bcc crystal, and x represents the number of Li/Na atoms adsorbed on group-VA monolayers.

3 Results and discussion

3.1 Single-layer antimonene

3.1.1 Single Li/Na atom adsorption. In the study of SL-Sb, a 4 × 4 antimonene supercell is used. As shown in Fig. 1(a), SL-Sb presents a wrinkle hexagonal honeycomb structure with a bond length of 2.87 Å (the upper Sb atoms are marked in red and the lower Sb atoms are marked in orange). The vertical distance between the red Sb atom and the orange Sb atom is d = 1.68 Å. The energy band and the DOS (density of states) of the pristine SL-Sb are calculated when Fermi level is set to 0 eV, as shown in Fig. 1(b) and (c), respectively. SL-Sb is an indirect bandgap semiconductor with a bandgap of 1.28 eV because the calculation may be underestimated by PBE method. This value is consistent with the previous research results (1.22 eV).[37]

Four possible adsorption sites are considered on the antimonene surface, as shown in Fig. 1(a). The H site represents the center of the hexagon, the V site is right above the lower Sb atom, the T site is right above the upper Sb atom, and the B site represents the middle position of two adjacent T sites. After relaxation, the optimal adsorption site of Li/Na is V. The Li atom placed at the T site moves to the H site, and placed at the B site moves to the V site. The Na atoms placed at the B and T sites move to the H sites after relaxation. Table 1 shows the vertical distance, adsorption distance, and adsorption energy and charge transfer of Li/Na at the V site. The maximum adsorption energy of Li is 1.91 eV, which is at the V site. The Li atom loses 0.99e, and the maximum charge gained by the adjacent Sb atoms is 0.28e. For Na atom adsorption, the maximum adsorption energy is 1.46 eV, which is also at the V site. The Na atom loses 0.99e, and the maximum charge gained by the adjacent Sb atoms is 0.29e. $d_{Sb\text{-}atom}$ represents the distance between Li/Na and the nearest neighbor Sb atom after relaxation, which is 2.81/3.19 Å. There is electrostatic interaction between Sb atoms and Li/Na atom due to charge transfer. The electrostatic interaction between Li and Sb is stronger because d_{Sb-Li} is smaller than d_{Sb-Na}, which results a larger adsorption energy of Li. $H_{Sb\text{-}atom}$ represents the vertical distance between Li/Na at the V site and the upper antimonene plane after relaxation, which is 1.58/2.18 Å. H_{Sb-Li} is smaller than H_{Sb-Na}, this is because Na is larger than Li. They tend to stay at the V sites to form bonds with more Sb atoms.

Fig. 2(a)/(e) is the energy band of SL-Sb adsorbing Li/Na at the V site. After adsorption of Li/Na, the valence band structure of pristine SL-Sb is primarily unchanged. The impurity band appears at the bottom of the conduction band, with the Fermi energy level passes through it. This shows that the electronic structure of the SL-Sb has transformed from semiconductor to metal. Good electrical conductivity is favorable for the use of antimonene as electrode of Li/Na ion batteries. Fig. 2(b)–(d) give the total DOS of Li adsorbed SL-Sb (Sb–Li), the partial density of states (PDOS) of Sb and of Li, respectively. Fig. 2(f)–(h) give the total DOS of Na adsorbed SL-Sb (Sb–Na), the PDOS of Sb and of Na, respectively. Comparing Fig. 2(b) and (f) with Fig. 1(c), the DOS of Sb–Li/Sb–Na is similar to that of pristine SL-Sb, but the Fermi level of Sb–Li/Sb–Na shifts to high energy direction. In Fig. 2(c) and (d), the s, p orbitals of Sb and the s, p orbitals of Li overlap at energy of −4.5, −2.8, −2.0, 0.3 and 0.7 eV, generating a series of resonance peaks, showing the characteristics of Li and Sb forming hybridized bonds. In Fig. 2(g) and (h), the s, p orbitals of Sb and of Na mainly overlap at energies of −4.5, −2.7, −2.0, −0.6 and 1.2 eV. It can be seen from the PDOS of Li/Na that the peak near the Fermi level is mainly originate from Li/Na atoms, which is consistent with the analysis of the energy band. Comparing the PDOS of Li and of Na, the electron states near the Fermi level of Sb–Li are mainly contributed by s and p orbitals of Li, while those near the Fermi level of Sb–Na are mainly contributed by s orbitals of Na. Because the size of Na is larger than Li, the extended s orbital of Na is more likely to form bond with Sb than p orbital.

In order to understand the charge redistribution of Li/Na adsorbed SL-Sb, the differential charge density of the adsorption system have been calculated and analyzed. Fig. 3(a) and (b) show the differential charge density of Sb–Li and of Sb–Na, respectively. The blue region is the charge consumption region, and the yellow region is the charge accumulation region. As shown in Fig. 3(a), when Li is at the V site, the electrons mainly transfers from Li to the nearest four Sb atoms. Except the Sb atom at the bottom, the six secondary nearest Sb atoms connected to the nearest three Sb atoms also obtain charges. In Fig. 3(b), Na has similar situation with Li at the V site. It

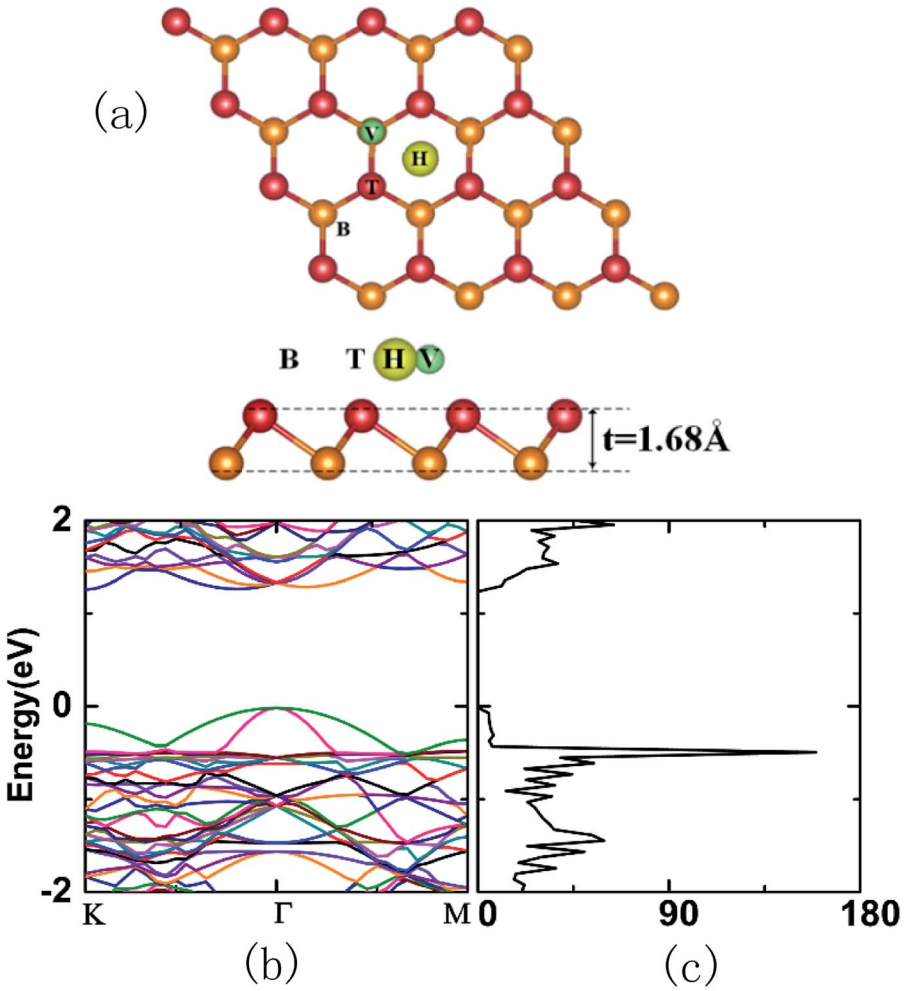

Fig. 1 (a) Geometric structure of SL-Sb (top view and side view) and several possible adsorption sites (the optimal adsorption site of Li/Na is V); (b) the energy band (the bandgap is about 1.28 eV) and (c) the DOS of SL-Sb. The red atoms represent Sb atoms in the upper layer, the orange atoms represent Sb atoms in the lower layer, the green atoms represent Li atoms, and the yellow atoms represent Na atoms (all the following antimonene structures and Li/Na atoms are marked in the same colors).

transfers electrons mainly to the four nearest Sb atoms, and to the secondly nearest six Sb atoms. The Li/Na atoms exchange charges with further Sb atoms, showing the non-locality of the interaction. Combined with the previous DOS analysis, it is shown that the bond between Sb and Li/Na has some metallic bond properties.

3.1.2 Multiple Li/Na atoms adsorption. The density of the ions stably adsorbed on the electrode can be used to measure the storage capacity of LIBs/NIBs. Therefore, we studied the stability of the SL-Sb adsorbed different densities of Li/Na. Fig. 4(a)–(d) give the initial and relaxed configurations of 3, 6, 16, and 32 Li atoms adsorbed SL-Sb at the V sites on one side and both sides, respectively. It can be seen that the SL-Sb is stable when adsorbing 3 Li atoms on one side, but the structure is deformed after other 3 Li are added on another side. For 16 Li adsorption on one side, as Fig. 4(c) shows, the structure decomposed. To balance the interaction between Li and SL-Sb, other 16 Li atoms are added to another side, as shown in Fig. 4(d), and the SL-Sb changed to an ordered alloy structure. According to the previously given equation, the average OCV of 3 Li atoms intercalated SL-Sb (Li_3Sb_{32}) is 0.37 V. The x value of Li_xSb is 0.094 which corresponding to Li_3Sb_{32}. The OCV value is consistent with other report.[44] Fig. 4(e)–(h) show the initial and relaxed configurations of 3, 6, 16, 32 Na atoms adsorbed SL-Sb at the V sites, respectively. In the configurations of 3 Na atoms

Table 1 Li/Na at four adsorption sites: adsorption energy (E), electron transfer (Δq), Li/Na–Sb distance ($d_{Sb\text{-}atom}$), vertical distance from Li/Na to Sb plane ($H_{Sb\text{-}atom}$)

			Bader (Δq)			
	$E_{H\text{-}site}$ (eV)	$E_{V\text{-}site}$ (eV)	Sb	V-site	$d_{Sb\text{-}atom}$ (Å)	$H_{Sb\text{-}atom}$ (Å)
Li	1.80	1.91	0.28	−0.99	2.81	1.58
Na	1.45	1.46	0.29	−0.99	3.19	2.18

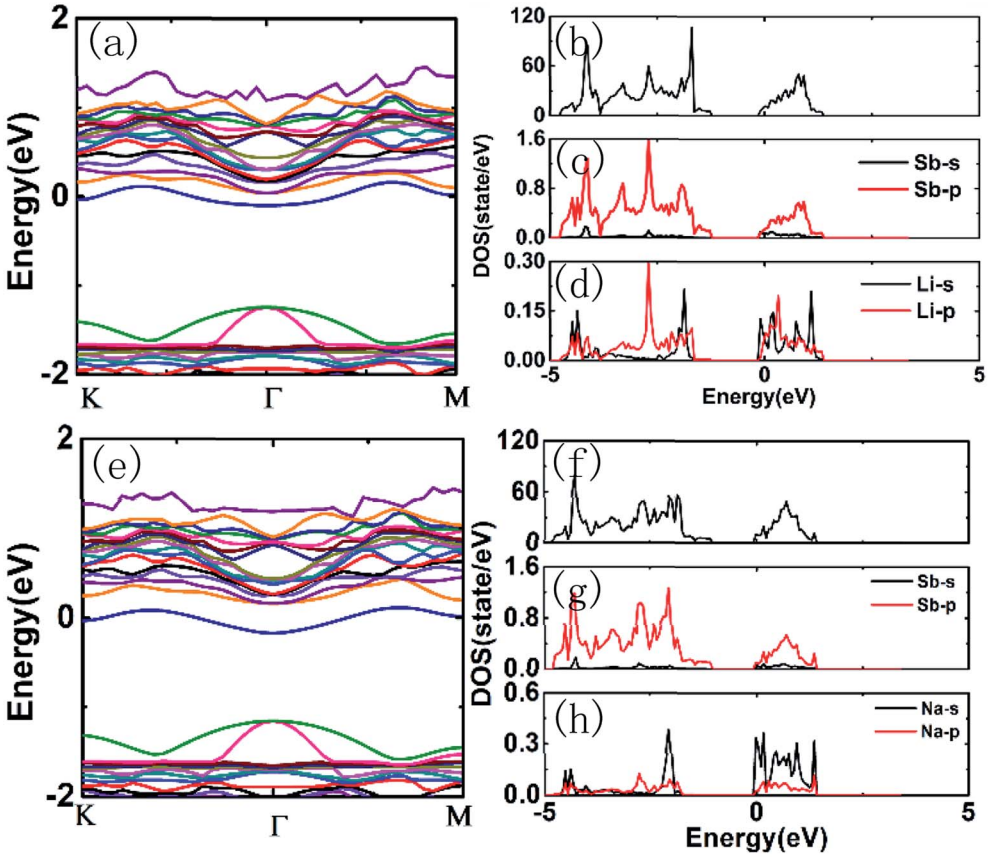

Fig. 2 SL-Sb adsorbs Li at V site: (a) the energy band, (b) the total DOS, the partial density of states (PDOS) of (c) Sb and of (d) Li; SL-Sb adsorbs Na at V site: (e) the energy band, (f) the total DOS, the PDOS of (g) Sb and of (h) Na.

adsorbed on one side and 6 atoms on two sides, the crystal structures of SL-Sb remain stable. However, after 16 Na are added on one side, the SL-Sb shows a tendency of alloying. When 32 Na atoms adsorb on both sides, the SL-Sb retains its original structure. The OCV of Na_3Sb_{32} and $Na_{32}Sb_{32}$ are 0.30 V and 0.26 V, respectively, showing the general trend of voltage reduction as the adsorption density increases.

Fig. 5(a) shows the DOS of 3, 16 and 32 Li atoms adsorbed SL-Sb (Sb–3Li, Sb–16Li and Sb–32Li). The DOS of Sb–3Li is similar to the DOS of the pristine SL-Sb. Besides the DOS peaks near the conduction band bottom and the valence band top of the pristine SL-Sb, two new DOS peaks appears in the −1.2 to 0 eV energy range of the Sb–3Li, and the Fermi energy level moves to the high-energy direction. The DOS of Sb–16Li changes notably, and the DOS curve become flattened, indicating that the electronic structure of the SL-Sb changes distinctly. For Sb–32Li, its DOS has also changed significantly, multiple DOS peaks appear in the −3.2 to 0 eV energy range. Fig. 5(b) shows the DOS of 3, 16 and 32 Na atoms adsorbed SL-Sb (Sb–3Na, Sb–16Na and Sb–32Na). The DOS of Sb–3Na is similar to that of the pristine SL-Sb, with the Fermi energy level moves to the high-energy direction. However, the DOS of Sb–16Na is very different from

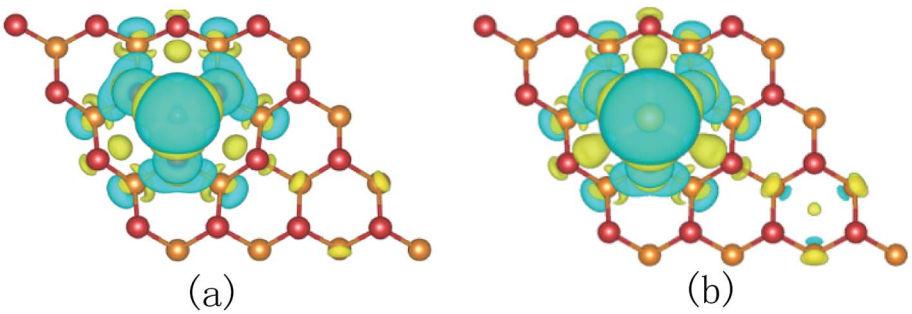

Fig. 3 The differential charge density of (a) Sb–Li (at the V site) and (b) Sb–Na (at the V site).

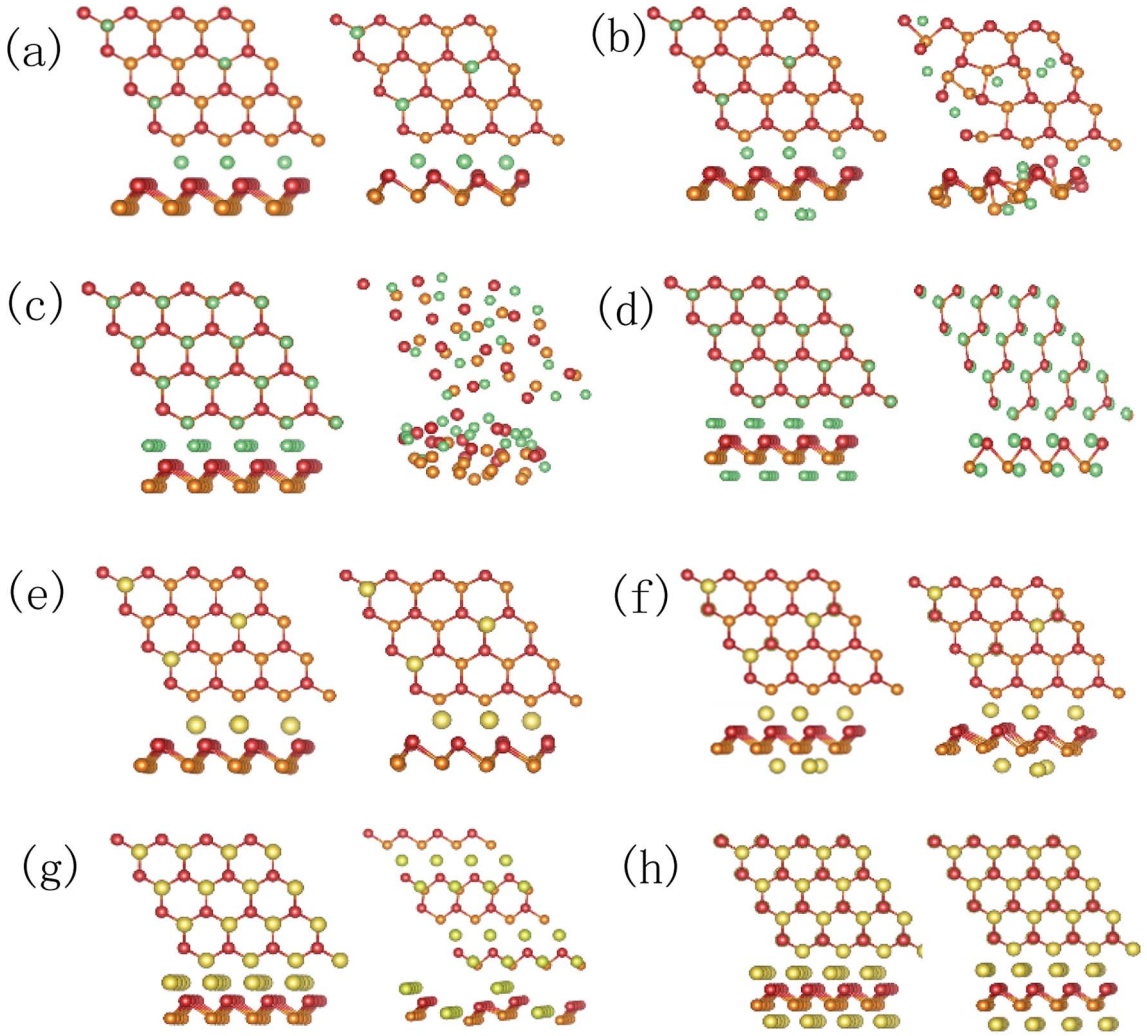

Fig. 4 The initial and relaxed configurations of (a) 3, (b) 6, (c) 16 and (d) 32 Li atoms adsorbed SL-Sb at the V site; the initial and relaxed configurations of (e) 3, (f) 6, (g) 16 and (h) 32 Na atoms adsorbed SL-Sb at the V site.

the DOS of the pristine SL-Sb, and multiple DOS peaks appear in the −3.5 to 0 eV energy range. However, after adsorption of 32 Na atoms, the antimonene maintains stable, therefore the DOS of Sb–32Na has a certain similarity with the DOS of the pristine SL-Sb. In contrast, when antimonene adsorbs 32 Li atoms on its two sides, its structure is disturbed, with the DOS significantly changed, showing a trend of forming alloy. It seems that the adsorption of Na on SL-Sb is more stable than that of Li.

3.2 Double-layer antimonene

3.2.1 Single Li/Na atom adsorption. Since few-layer antimonene is more likely to be used as actual electrode material, we built a double-layer antimonene (DL-Sb) model as the representative to study Li/Na adsorption on few-layer antimonene. As shown in Fig. 6(a), a 3 × 3 DL-Sb supercell containing 36 Sb atoms is built. The upper and lower Sb atoms of each layer of DL-Sb are represented by red and orange atoms, respectively. The distance between two layers of DL-Sb is 2.43 Å, and the bond length between two Sb atoms is 2.92 Å. As shown in Fig. 6(b) and (c), the energy band and the DOS of DL-Sb are calculated where Fermi energy level is set to 0 eV. Compared with SL-Sb, the band gap of DL-Sb decreases to 0 eV. When single layer changes to double layer, antimonene transforms from semiconductor to semi-metal, which is consistent with the results reported in Zhang's paper.[26]

As shown in Fig. 6(a), we consider four adsorption sites in DL-Sb. The H1 site represents the hexagonal center outside DL-Sb layer, and the V1 site is the valley position. The H2 site is the hexagonal center in the interlayer, and the V2 site is the valley position. Table 2 shows the adsorption energy and charge transfer of Li/Na on DL-Sb. It can be seen that the V2 site is the most stable position of Li adsorption, with adsorption energy of 2.71 eV. Li loses 1*e* at the V2 site, primarily transferring electrons to the eight close Sb atoms, and the maximum charge gained by the adjacent Sb atoms is 0.13*e*. The most stable position of Na adsorption is the V1 site, with adsorption energy of 1.72 eV. The Na atom placed at the H2 site undergoes relaxation and finally returns to the V2 site. Na loses 1*e* at the V1 site,

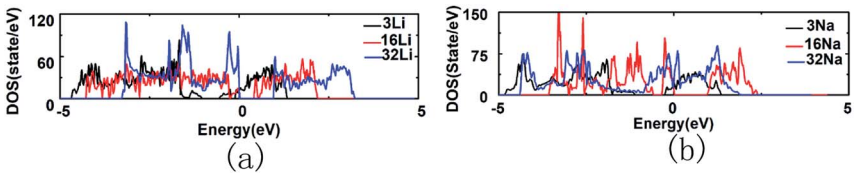

Fig. 5 (a) The DOS of SL-3Li and SL-9Li; (b) the DOS of SL-3Na and SL-9Na.

primarily transferring electrons to the nearest three Sb atoms, and the maximum charge gained by the adjacent Sb atoms is 0.28*e*. Li tends to adsorb in the DL-Sb interlayer, while Na is more likely to adsorb on the outside of DL-Sb. Similar to the previous analysis, the size of Li is relatively small, therefore it can be accommodated in the DL-Sb interlayer and interacts with more Sb atoms. As Na is relatively large, it is difficult to be inserted into the DL-Sb interlayer, and that is the reason why Na tends to adsorb outside the surface.

Fig. 7(a) is the energy band of Li adsorbed DL-Sb at the V2 site, and Fig. 7(e) is the energy band of Na adsorbed DL-Sb at the V1 site. Similar to the analysis of SL-Sb, the valence band of DL-

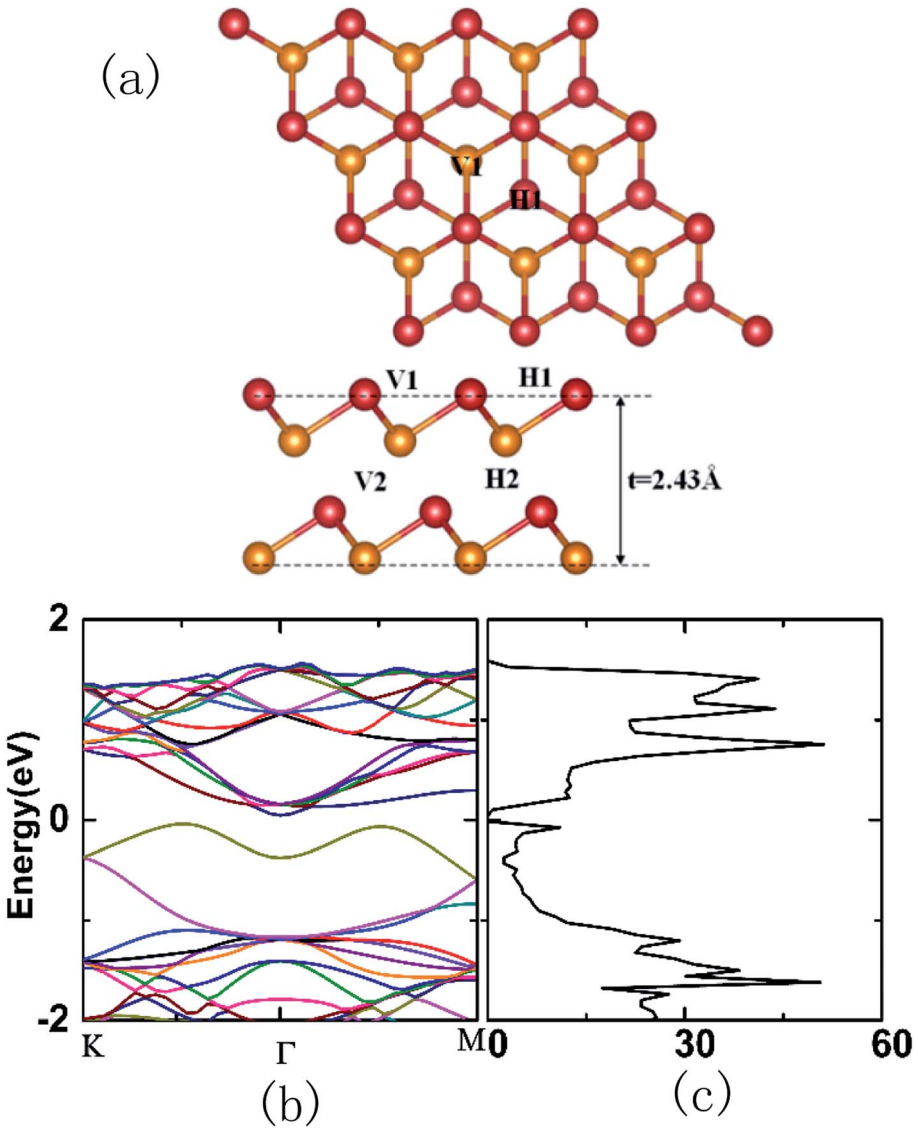

Fig. 6 (a) The structure of DL-Sb and four possible adsorption sites. H1 and V1 represent adsorption sites on the outside of the DL-Sb; H2 and V2 represent adsorption sites in the DL-Sb interlayer. The optimal adsorption site of Li/Na on the DL-Sb is V2/V1. (b) The energy band structure and (c) the DOS of the pristine DL-Sb.

Table 2 Li/Na at four adsorption sites: adsorption energy (E), electron transfer (Δq)

					Bader (Δq)	
	E_{H1} (eV)	E_{V1} (eV)	E_{H2} (eV)	E_{V2} (eV)	Sb	Li/Na
Li	2.10	2.24	2.09	2.71	0.13	−1.00 (V2)
Na	1.70	1.72	1.60	1.60	0.28	−1.00 (V1)

Sb does not change significantly after adsorbing Li/Na, while the impurity band appears at the bottom of the conduction band. The Fermi level pass through the impurity band, showing that the Li/Na adsorption DL-Sb has metallicity. Fig. 7(b)–(d) show the DOS of Li adsorbed DL-Sb (2Sb–Li), the PDOS of Sb and of Li, respectively. Fig. 7(f)–(h) show the DOS of Na adsorbed DL-Sb (2Sb–Na), the PDOS of Sb and of Na, respectively. Comparing Fig. 7(b) and (f) with Fig. 6(c), it can be seen that the DOS of the 2Sb–Li/2Sb–Na is similar to the DOS of the pristine DL-Sb. Besides, a new DOS peak appears at −0.55 eV in the DOS of 2Sb–Na. In Fig. 7(c) and (d), the s orbital of Sb, and the s, p orbitals of Li hybridized to form a series of resonance peaks, showing that Li and Sb are hybridizing into bonds. Fig. 7(g) and (h) show the same hybridized characteristics of Na adsorbed DL-Sb.

Fig. 8(a) and (b) respectively shows the differential charge density of Li and of Na adsorbed DL-Sb at the V2 sites. The blue region is the charge consumption region, and the yellow region is the charge accumulation region. Li loses electrons, while the charge accumulates among Li and the surrounding eight Sb atoms. Na loses electrons, and the charge primarily accumulates closing to the eight Sb atoms. The differential charge density of Li/Na adsorbed on outside surface of DL-Sb is similar to that of SL-Sb.

3.2.2 Multiple Li/Na atoms adsorption. Fig. 9(a)–(c) show the initial and relaxed configurations of 9, 18 and 27 Li atoms adsorbed DL-Sb, respectively. Firstly, 9 Li atoms were placed at the V2 sites, the adsorbed DL-Sb was stable after relaxation. The OCV of DL-Sb adsorption 9 Li ation is 1.01 V, which is larger than the SL-Sb adsoption. This is because the stronger adsorption of DL-Sb. Then, 9 Li atoms were added to the V1 sites successively on the outside surface of DL-Sb. It is found that Li atoms were orderly inserted into the antimonene, and the pristine antimonene structure is completely distorted. Finally, another 9 Li atoms were added to the V1 sites on the contrary side, it could be seen that after relaxation, Li atoms on both surface of DL-Sb are bonded orderly with adjacent Sb atoms to

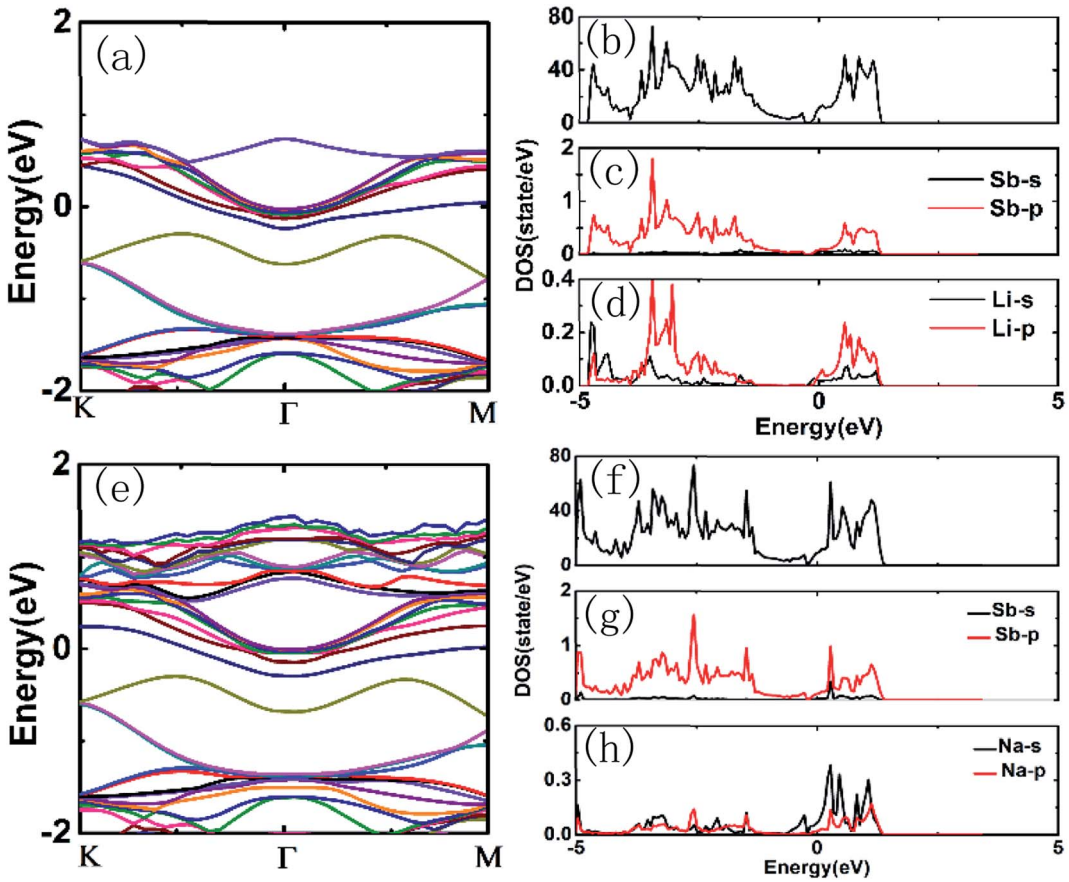

Fig. 7 DL-Sb adsorbs Li at the V2 site: (a) energy band, (b) DOS, (c) partial density of states (PDOS) of Sb and (d) PDOS of Li; DL-Sb adsorbs Na at the V1 site: (e) band, (f) DOS, (g) PDOS of Sb and (h) PDOS of Na.

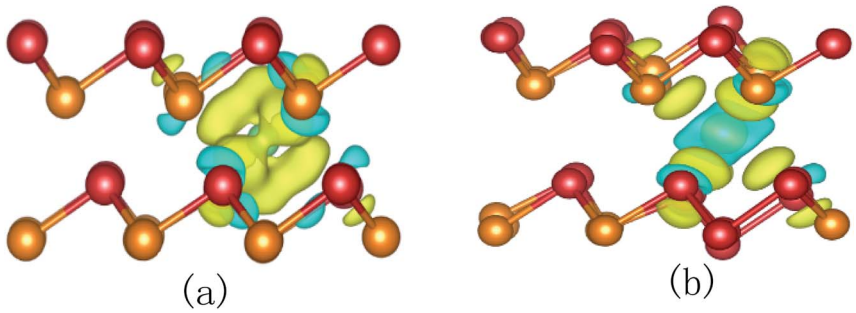

Fig. 8 The differential charge density of (a) 2Sb–Li and (b) 2Sb–Na. Both of Li and Na are at the V2 sites.

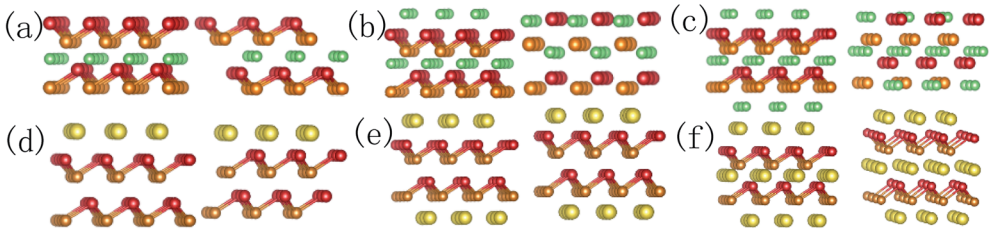

Fig. 9 The initial and relaxed configurations: DL-Sb adsorbs (a) 9, (b) 18 and (c) 27 Li atoms; DL-Sb adsorbs (d) 9, (e) 18 and (f) 27 Na atoms.

form alloy structures. Fig. 9(d)–(f) show the initial and relaxed configurations of 9, 18 and 27 Na atoms adsorbed DL-Sb, respectively. The DL-Sb is stable when 9 Na atoms were placed at the V1 sites on the outside surface of DL-Sb. Successively adding 9 Na atoms to V1 sites on another surface, the DL-Sb remains stable. Additional 9 Na atoms were added to the V2 sites in the interlayer of DL-Sb, the distance between two layers increased, but the DL-Sb still maintained its original structure. After 27 Na were intercalated in DL-Sb, which is corresponding to x value of 0.75 ($Li_{0.75}Sb$), the calculated average OCV is around 0.7 V. This value is larger than SL-Sb because of the stronger adsorption of Na on DL-Sb than SL-Sb. In summary, the adsorption of a small amount of Li atoms on DL-Sb is more stable than that on SL-Sb. With the increase of Li adsorption density, the structure tends to form alloy. However, the DL-Sb can maintain its original structure with the increase of Na adsorption density, which is very stable.

Fig. 10(a) shows the DOS of 9 Li atoms adsorbed DL-Sb (2Sb–9Li) and 27 Li atoms adsorbed DL-Sb (2Sb–27Li). The DOS of 2Sb–9Li is not significantly different from the DOS of pristine DL-Sb. However, compared with the DL-Sb, the DOS curve of 2Sb–27Li loses its original shape, and electronic structure changes fundamentally. Fig. 10(b) shows the DOS of 9 Na atoms adsorbed DL-Sb (2Sb–9Na) and 27 Na atoms adsorbed DL-Sb (2Sb–27Na), which are similar to the DOS of DL-Sb, while the Fermi energy level moves towards the high-energy direction. In summary, with the increase of Li adsorption density, the electronic structure of the DL-Sb has changed greatly. DL-Sb adsorbs Li atoms has a tendency to form alloy, while DL-Sb adsorbing the same density of Na atoms remains stable.

3.3 Li/Na diffusion

The charge and discharge rate of the battery are influenced by the conductivity and ion diffusion characteristics of the electrode material. The low diffusion barrier facilitates the insertion/extraction of ions in the electrode material and improves the charge and discharge speed. Herein, the diffusion characteristics of Li/Na on the SL-Sb and DL-Sb were investigated. Firstly, the diffusion of Li/Na on the surface of SL-Sb was investigated. Because the most stable adsorption site of Li/Na on the surface of SL-Sb is V, we set two adjacent V sites as the starting and ending positions of Li/Na diffusion. After NEB calculation, it is found that Li/Na atom will preferentially pass

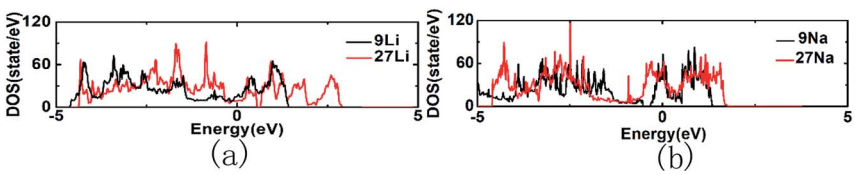

Fig. 10 (a) The DOS of 2Sb–9Li and 2Sb–27Li; (b) the DOS of 2Sb–9Na and 2Sb–27Na.

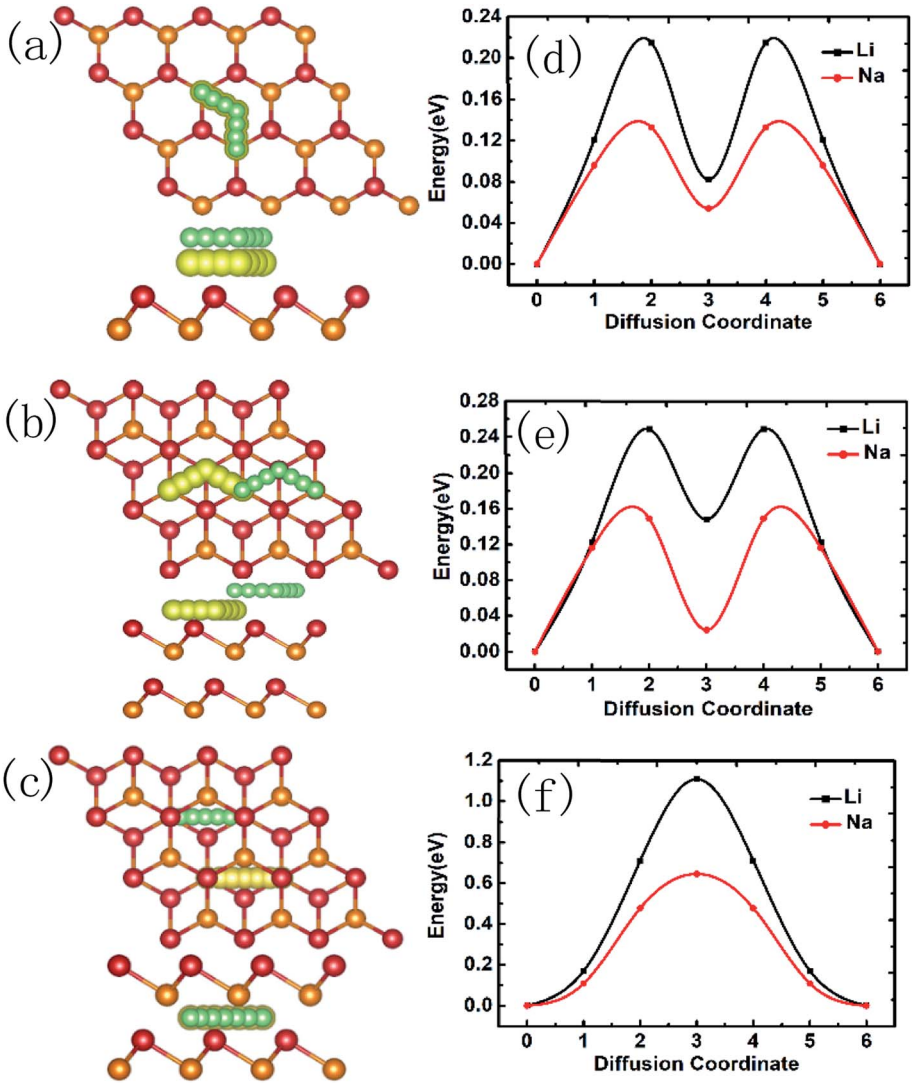

Fig. 11 (a) Diffusion path on the SL-Sb surface. Li/Na is from V to V, passing H. (b) Diffusion path on the DL-Sb surface. Li/Na is from V1 to V1, passing H1. (c) Diffusion path in the DL-Sb interlayer. Li/Na is from V2 to V2, along the straight line. (d)–(f) Corresponding diffusion barriers of (a)–(c), respectively.

through H site when it diffuses between two neighboring V sites, and Na atom will pass through a V site when diffusing between two neighboring H sites, as shown in Fig. 11(a). The diffusion barrier of Li/Na is 0.22/0.13 eV, as shown in Fig. 11(d). Na has a very small diffusion barrier on the surface of SL-Sb, thus Na is easier to diffuse on the surface of SL-Sb than Li. Because the Sb atoms in antimonene have lone pair electrons, when Li and Na adsorb on antimonene, they bind with the lone pair electron. This is the so-called cation–π interaction, which has the interaction energies decrease in the following order: $Mg^{2+} > Ca^{2+} > Li^{+} > Na^{+} > K^{+}$, resulting in weaker interaction of antimonene with Na than Li.[54,55] Therefore, the diffusion barriers for Na migration are always lower than that for Li.

The diffusion of Li/Na on the DL-Sb outside surface is similar to that of SL-Sb surface. The diffusion path of Li/Na is still V1–H1–V1, as shown in Fig. 11(b). However, the diffusion barrier of Li/Na on the DL-Sb surface is higher than that on the SL-Sb, which is 0.25/0.15 eV, as shown in Fig. 11(e). This is influenced by the interaction between two layers of the DL-Sb. Fig. 11(c) is the diffusion path of Li/Na moving from one V2 site along the straight line to the adjacent V2 site in the DL-Sb interlayer. The diffusion barrier of Li/Na is 1.11/0.65 eV, as shown in Fig. 11(f). The diffusion barrier on DL-Sb is higher than that on SL-Sb, which is due to the stronger adsorption of Li/Na atom on DL-Sb. For comparison, the calculated diffusion energy barriers of Li/Na on the SL-Sb/DL-Sb antimonene and other studied 2D-monolayer materials are listed in Table 3. The energy barriers of Li/Na on the surfaces of SL-Sb and DL-Sb are consistent with the previous result. The diffusion barriers of Li/Na on the surfaces of DL-Sb and the SL-Sb are relatively low, while they are relatively higher in the DL-Sb interlayer. Comparing Li and Na, Na has a lower diffusion barrier on SL-Sb and DL-Sb (especially outside the DL-Sb surface), which means

Table 3 Diffusion energy barriers ΔE of some 2D monolayer materials and SL-Sb/DL-Sb in our work

2D material (monolayer)	ΔE for Li (eV)	ΔE for Na (eV)
Black phosphorene	0.08;[45] 0.12 (ref. 20)	0.04;[46] 0.04 (ref. 21)
Blue phosphorene	0.14;[44] 0.16 (ref. 20)	0.07 (ref. 44)
Borophene	0.025;[47] 0.0026 (ref. 48)	0.003 (ref. 47)
Graphene	0.22;[49] 0.31;[50] 0.38 (ref. 10)	0.14 (ref. 10)
Silicene	0.35;[10] 0.23;[51] 0.25 (ref. 52)	0.23;[10] 0.16;[53] 0.14 (ref. 8)
Germanene	0.25 (ref. 8)	0.16 (ref. 8)
Stanene	0.25 (ref. 8)	0.16 (ref. 8)
β-Antimonene	0.25;[44] 0.337 (ref. 38)	0.14;[44] 0.114 (ref. 38)
SL-Sb	0.22	0.13
DL-Sb (outside)	0.25	0.15
DL-Sb (inside)	1.11	0.65

Na atoms have faster diffusion rate then Li atoms on antimonene.

4 Conclusion

The adsorption characteristics of Li/Na atoms on SL-Sb and DL-Sb have been studied. The optimal adsorption position of Li/Na atom on SL-Sb is V site with the adsorption energy of 1.91/1.46 eV. With the increase of Li atoms adsorption density, the crystal structure of the antimonene is deformed, and the DOS of the adsorbed SL-Sb changes significantly. While the antimonene retains its original structure when adsorbing 32 Na, and the DOS of the adsorption system is similar to that of pristine SL-Sb.

Li atom has the maximum adsorption energy of 2.71 eV at the V2 site in the interlayer of DL-Sb, and Na atom has the maximum adsorption energy of 1.72 eV at the V1 site on the DL-Sb outside surface. With the increases of Li adsorption density, the crystal structure and the electronic structure of the DL-Sb change significantly, showing a trend of forming alloy. In contrast, with the increases of Na adsorption density, the crystal structure remains stable, and the DOS still maintain similar characteristics of the pristine DL-Sb. Compared with the SL-Sb, the DL-Sb is more stable in Li/Na atoms adsorption.

In addition, the diffusion behaviors of Li/Na on SL-Sb and DL-Sb have also been studied. The diffusion path of Li/Na on SL-Sb is V–H–V with diffusion barrier of 0.22/0.13 eV. The diffusion path of Li/Na outside the DL-Sb layer is the same as that on the SL-Sb surface, but the diffusion barrier is 0.25/0.15 eV, which is larger than SL-Sb. In the interlayer, Li/Na atom moves from the V2 site along the straight line to the adjacent V2 site, and the energy barrier is 1.11/0.65 eV. The diffusion barrier of Na is lower than that of Li, because the adsorption energy of Li atoms on antimonene is larger than that of Na atoms.

In summary, the double-layer antimonene is much stable than single-layer antimonene in Li/Na adsorption. In particular, DL-Sb can maintain its layered structure with larger adsorption density of Na atoms. The diffusion barrier of Li/Na atoms on the surface of the antimonene is low, which is beneficial to the rapid charge and discharge of anode. Therefore, all of the characteristics suggest that the few-layer antimonenes are promising candidates for anode materials of LIBs/NIBs.

Conflicts of interest

There are no conflicts to declare.

Acknowledgements

The authors acknowledge the support of the National Natural Science Foundation of China (Grant No. 61372050) and double-first-rate construction project in NCEPU (No. 1907423).

References

1 J. M. Tarascon and M. Armand, *Nature*, 2001, **414**, 359–367.
2 J. Sun, G. Zheng, H. W. Lee, *et al.*, *Nano Lett.*, 2014, **14**, 4573–4580.
3 N. Yabuuchi, K. Kubota, M. Dahbi, *et al.*, *Chem. Rev.*, 2014, **114**, 11636–11682.
4 X. F. Yu, G. Giorgi, H. Ushiyama, *et al.*, *Chem. Phys. Lett.*, 2014, **612**, 129–133.
5 K. Rytkönen, J. Akola and M. Manninen, *Phys. Rev. B: Condens. Matter Mater. Phys.*, 2004, **69**, 1324–1332.
6 R. Alcántara, J. Mateos, M. Juan, *et al.*, *Electrochem. Commun.*, 2001, **3**, 639–642.
7 L. Wei, S. Fei, C. Bommier, *et al.*, *Acc. Chem. Res.*, 2016, **49**, 231–240.
8 B. Mortazavi, A. Dianat, G. Cuniberti, *et al.*, *Electrochim. Acta*, 2016, **213**, 865–870.
9 L. Baggetto, P. Ganesh, R. P. Meisner, *et al.*, *J. Power Sources*, 2013, **234**, 48–59.
10 L. Shi, T. S. Zhao, A. Xu, *et al.*, *J. Mater. Chem. A*, 2016, **4**, 16377–16382.
11 E. J. Yoo, J. Kim, E. Hosono, *et al.*, *Nano Lett.*, 2008, **8**, 2277–2282.
12 J. Zheng, Z. Ren, P. Guo, *et al.*, *Phys. Chem. Chem. Phys.*, 2014, **16**, 10419–10424.
13 C. Ling and F. Mizuno, *Phys. Chem. Chem. Phys.*, 2014, **16**, 10419–10424.
14 C. Chen, Y. Wen, X. Hu, *et al.*, *Nat. Commun.*, 2015, **6**, 6929.
15 L. Shi, T. S. Zhao, A. Xu, *et al.*, *Sci. Bull.*, 2016, **61**, 1138–1144.
16 Y. Zhang, Z. F. Wu, P. F. Gao, *et al.*, *ACS Appl. Mater. Interfaces*, 2016, **8**, 22175.

17 A. J. Mannix, X. F. Zhou, B. Kiraly, *et al.*, *Science*, 2015, **350**, 1513–1516.
18 Y. Huang, C. Zhu, S. Zhang, *et al.*, *Nano Lett.*, 2019, **19**, 1118.
19 S. Zhao, W. Kang and J. Xue, *J. Mater. Chem. A*, 2014, **2**, 19046–19052.
20 Q. F. Li, C. G. Duan, X. G. Wan, *et al.*, *J. Phys. Chem. C*, 2015, **119**, 8662–8670.
21 X. Liu, Y. Wen, Z. Chen, *et al.*, *Phys. Chem. Chem. Phys.*, 2015, **17**, 16398–16404.
22 K. P. S. S. Hembram, H. Jung, B. C. Yeo, S. J. Pai, *et al.*, *Phys. Chem. Chem. Phys.*, 2015, **119**, 15041–15046.
23 K. P. S. S. Hembram, H. Jung, B. C. Yeo, S. J. Pai, *et al.*, *Phys. Chem. Chem. Phys.*, 2016, **18**, 21391–21397.
24 A. C. Gomez, L. Vicarelli, E. Prada, *et al.*, *2D Materials*, 2014, **1**, 025001.
25 J. O. Island, *et al.*, *2D Materials*, 2015, **2**, 011002.
26 S. Zhang, Z. Yan, Y. Li, Z. Chen and H. Zeng, *Angew. Chem.*, 2015, **127**, 3155–3158.
27 S. Zhang, M. Xie, F. Li, *et al.*, *Angew. Chem.*, 2016, **128**, 1698–1701.
28 C. Huo, X. Sun, Z. Yan, *et al.*, *J. Am. Chem. Soc.*, 2016, **139**, 3568.
29 C. Gibaja, D. Rodriguean, *et al.*, *Angew. Chem., Int. Ed.*, 2016, **55**, 14470.
30 G. Abellan, *et al.*, *ChemInform*, 2016, **47**, DOI: 10.1002/chin.201652019.
31 Y. J. Gao, W. Tian, *et al.*, *J. Mater. Chem. A*, 2019, **7**, 3238–3243.
32 T. Lei, C. Liu, J. L. Zhao, *et al.*, *J. Appl. Phys.*, 2016, **119**, 015302.
33 S. Guo, Y. Zhang, *et al.*, *Adv. Mater.*, 2019, 1902352.
34 S. Zhang, S. Guo, *et al.*, *Chem. Soc. Rev.*, 2018, **47**, 982–1021.
35 J. He, Y. Wei, T. Zhai, *et al.*, *Mater. Chem. Front.*, 2018, **2**, 437–455.
36 J. Qian, Y. Chen, L. Wu, *et al.*, *Chem. Commun.*, 2012, **48**, 7070–7072.
37 F. Zhang, W. Li and X. Dai, *Superlattices Microstruct.*, 2016, **100**, 826–836.
38 A. Sengupta and T. Frauenheim, *Mater. Today Energy*, 2017, **5**, 347–354.
39 G. Kresse, J. Furthmüller, *et al.*, *Phys. Rev. B: Condens. Matter Mater. Phys.*, 1996, **54**, 11169–11186.
40 G. Kresse, J. Furthmüller, *et al.*, *Comput. Mater. Sci.*, 1996, **6**, 15–50.
41 T. Bučko, J. Hafner, S. Lebègue and J. G. Ángyán, *J. Phys. Chem. A*, 2010, **114**, 11814–11824.
42 S. Karmakar, C. Chowdhury, A. Datta, *et al.*, *J. Phys. Chem. C*, 2016, **120**, 14522–14530.
43 D. Er, J. Li, M. Naguib, Y. Gogotsi, *et al.*, *ACS Appl. Mater. Interfaces*, 2014, **6**, 11173–11179.
44 S. Guo, *et al.*, *J. Phys. Chem. C*, 2018, **122**, 29559–29566.
45 W. Li, Y. Yang, G. Zhang and Y. W. Zhang, *Nano Lett.*, 2015, **15**, 1691–1697.
46 V. V. Kulish, O. I. Malyi, C. Persson and P. Wu, *Phys. Chem. Chem. Phys.*, 2015, **17**, 13921–13928.
47 B. Mortazavi, A. Dianat, O. Rahaman, G. Cuniberti and T. Rabczuk, *J. Power Sources*, 2016, **329**, 456–461.
48 H. R. Jiang, Z. Lu, M. C. Wu, F. Ciucci and T. S. Zhao, *Nano Energy*, 2016, **23**, 97–104.
49 K. Persson, Y. Hinuma, Y. S. Meng, A. Van der Ven and G. Ceder, *Phys. Rev. B: Condens. Matter Mater. Phys.*, 2010, **82**, 125416.
50 X. Fan, W. T. Zheng and J. L. Kuo, *ACS Appl. Mater. Interfaces*, 2012, **4**, 2432–2438.
51 G. A. Tritsaris, E. Kaxiras, S. Meng and E. Wang, *Nano Lett.*, 2013, **13**, 2258–2263.
52 J. Setiadi, M. D. Arnold and M. J. Ford, *ACS Appl. Mater. Interfaces*, 2013, **5**, 10690–10695.
53 J. Zhu and U. Schwingenschlögl, *2D Mater.*, 2016, **3**, 035012.
54 S. A. Abraham, D. Jose and A. Datta, *ChemPhysChem*, 2012, **13**, 695–698.
55 A. S. Mahadevi and G. N. Sastry, *Chem. Rev.*, 2013, **113**, 2100–2138.